



Crashworthiness capability comparison of a 3D Greek cross fractal structure additively manufactured with polyamide and thermoplastic polyurethane

Marco Viccica · Gabriel Ferreira Serra ·
Ricardo Alves de Sousa · Manuela Galati

Received: 13 December 2023 / Accepted: 30 April 2024
© The Author(s) 2024

Abstract Designers are continuously searching for materials or meta-structures, also inspired by nature, that exhibit favourable strength-to-weight ratios, substantial heat transfer capabilities, and efficient energy absorption. One particular example includes fractal geometries, which usually consist of intricate three-dimensional geometrical structures and are challenging to produce through traditional manufacturing methods. In this regard, this study analyses the performance of a three-dimensional cross-based fractal structure (3D-CFS) designed for energy absorption and manufactured using polymeric materials. Mathematically, the geometry is obtained using a 3D Greek cross repeated in the 3D space according to the fractal principle. Owing to the intricate final structure, samples are fabricated using an Additive Manufacturing system based on powder bed fusion with a laser beam and infrared light. The study is carried out using two

polymeric materials, polyamide and thermoplastic polyurethane, and the mechanical response of the structure is analysed under dynamic compression tests. The tested geometries consisted of samples with a single 3D-CFS cell, various volume fractions and a configuration with multiple cells that emulated a possible layout for linear helmet application. The findings indicate that the 3D-CFS is a promising geometry for eventual implementation into shock absorption applications, specifically in personal protective equipment (PPE) usage.

Keywords Fractal · TPU · PBF-IrL · PA12 · PBF-LB/P · PPE · Shock absorption

1 Introduction

In recent years, additive manufacturing (AM) development has opened new design opportunities toward optimised and enhanced structural components in many different engineering areas. Specifically, the advancement of AM techniques and the implementation of mathematical and bio-inspired geometries have drastically accelerated the progress of impact absorber devices with superior efficiency, particularly for personal protective equipment (PPE) applications. In this context, extensive research explored the crashworthiness characteristics of liner helmets in military [1] and sports [2, 3] fields. The principal aim is to reduce the weight while increasing the effectiveness

Supplementary Information The online version contains supplementary material available at <https://doi.org/10.1007/s11012-024-01818-x>.

M. Viccica (✉) · M. Galati
Integrated Additive Manufacturing Center (IAM),
Department of Management and Production Engineering
(DIGEP), Politecnico di Torino, Turin, Italy
e-mail: marco.viccica@polito.it

G. F. Serra · R. A. de Sousa
Centre for Mechanical Technology and Automation
(TEMA), Department of Mechanical Engineering,
University of Aveiro, Aveiro, Portugal

of the helmet. Periodic cellular structures, based on struts [4, 5] or surfaces [6–8] and fabricated using additive manufacturing technologies, are suitable options for decreasing the peak linear acceleration (PLA) of a helmeted head significantly. Therefore, these geometries are considered good candidates to replace liner materials, namely expanded polystyrene (EPS) [9]. Similarly, fractal geometry [10–12] and bio-inspired shapes [13, 14] have been demonstrated to be characterised by impressive cushioning properties. However, the application of such structures has been inhibited by the difficulties of fabricating such irregular, intricate, and self-similar three-dimensional characteristics. Few examples reported in the literature show how to overcome this issue using AM technologies. Concerning impact absorption, to the best of the authors' knowledge, only one work [15] has been carried out on a single fractal cell based on a 3D Greek cross manufactured using polyamide 12 (PA12). The structure has been tested under quasi-static compression loads. This structure has shown up to 77% higher specific energy absorption than a conventional EPS foam.

Owing to this promising preliminary result, this work is a detailed and extended version of Viccica et al. [16] investigating the 3D cross-based fractal structure (3D-CFS) capabilities toward the testing under high strain-rate compression loads. Here, structures were designed by varying the volume fraction, and the performances of the most common PA12 were compared to those of thermoplastic polyurethane (TPU). A configuration including multiple cells was also introduced to test a prototype closer to an actual application in linear helmets for personal protective equipment head protection.

2 Materials and methods

2.1 Greek cross-based fractal design

3D-CFS is designed by subsequently replicating and scaling a three-dimensional Greek cross initiator. Figure 1a illustrates the initiator shaped by three equal beams, obtained extruding, for a certain length, L , a circular section of diameter D along the axes of the cartesian frame. The third iteration (Fig. 1a) represents the elementary structure, which is repeated in the 3D space 15 times around a central structure to

obtain a sufficient domain to extract the so-defined elementary cell (Fig. 1b, each repetition is indicated with a different colour). Each elementary structure is adjacent to another and aligned to the vertexes of the structures without compenetrating so that the repetitions form a single continuous structure. From the obtained arrangement, the elementary cell for the testing is then obtained by cutting the structure in Fig. 1b using planes (Fig. 1c) perpendicular to and passing through the extremities of the three beams composing the initial initiator (Fig. 1a, 1st iteration). The extracted portion, called 3D-CFS, is reported in Fig. 1d, while the final structure for the testing is represented in Fig. 1e and includes two plates parallel to each other and perpendicular to one of the beams composing the initial initiator.

The global dimension and the volume fraction (VF) of the 3D-CFS are parametric and determined by two primary geometric parameters at the initial iteration: the strut length L and diameter D . The VF parameters represent the portion of the volume occupied by the structure in comparison with the overall dimensions of the structure. To analyse the effect of VF on the mechanical performance, three configurations have been chosen. The diameter of the initiator has been set higher than 1.5 mm to avoid drastic drops in structural stiffness because of the appearance of manufacturing defects [15]. Each design is indexed with an alphanumeric code in which the letter precedes a number and identifies the variables (length, L or diameter, D). The number indicated the measure of the corresponding variable, expressed in mm. As an example, L40_D2.0 identifies an initiation with length L equal to 40 mm, and a diameter D equal to 2 mm. The configurations are the following:

- L40_D2.0, resulting in a volume fraction VF equal to 9.1%. This configuration corresponds to the one reported in Ref. [15]
- L28_D1.8, resulting VF = 14.1%
- L28_2.0, resulting VF = 16.8%
- L20_D1.6, resulting VF = 20.1%.

The variation of the two parameters provides a comprehensive evaluation of the VF effect on the mechanical response of the structure. In addition, the analysis of the configurations with $L=28$ mm allows to investigate the main impact of the diameter on the mechanical response of the structure.

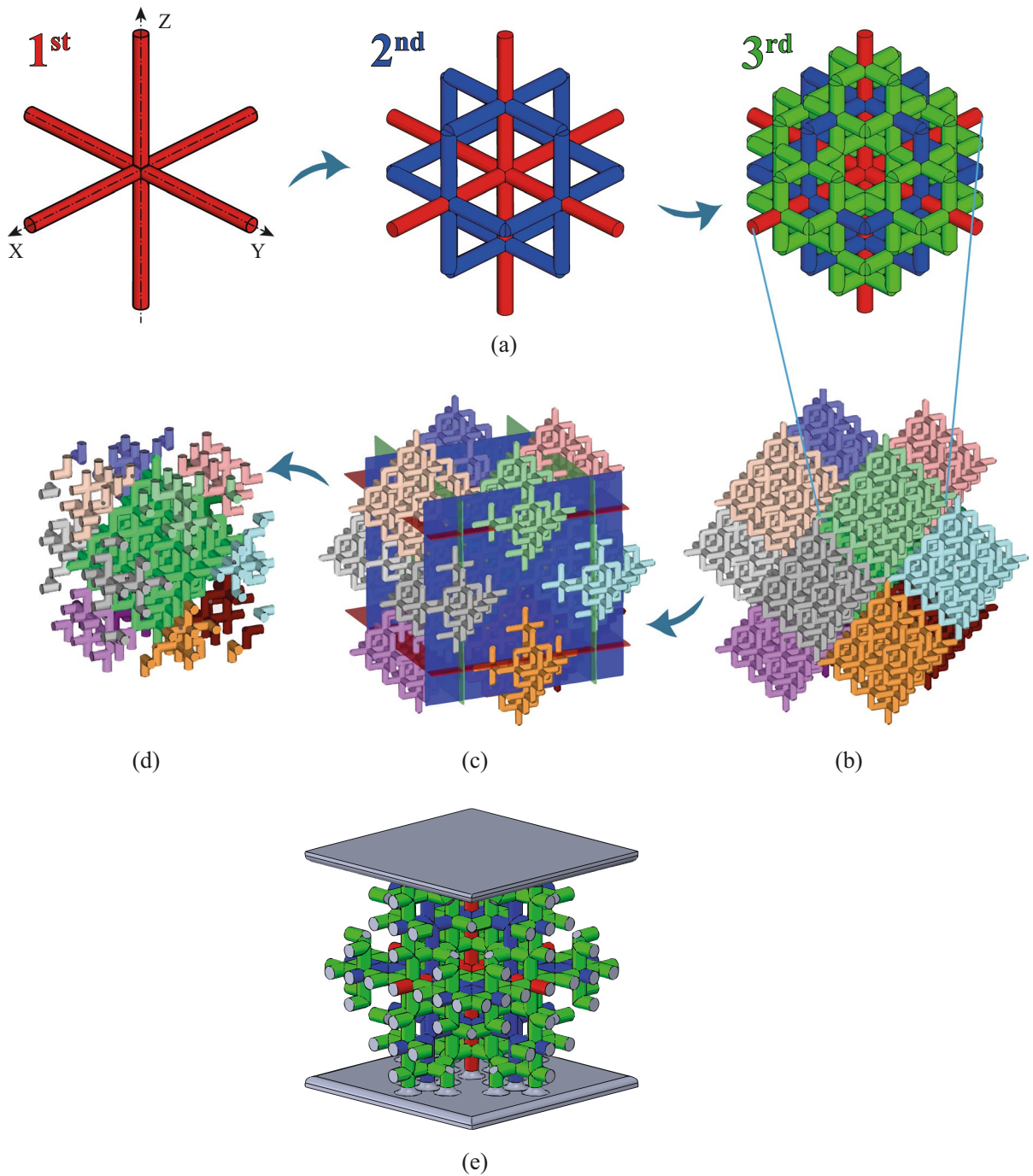


Fig. 1 **a** 3D-CFS iterations: in red, the first step; in blue and green, the added axes of the second and third steps, respectively; **b** replication of the single structure in a 3D space, each repetition is indicated with a different colour; **c** cutting planes

for obtained the cubic structure for the testing; **d** extracted cubic portion, 3D-CFS; **e** sample for the testing consisting of 3D-CFS and two parallel plates for the load application cubic compression sample

2.2 Production and testing

The materials analysed are two polymers that are characterised by substantially different properties: thermoplastic polyurethane (TPU) and polyamide 12 (PA12) (Table 1). All samples were built using AM powder bed fusion systems. These systems operate by distributing a thin layer of powder on the build platform and selectively sintering the powder material according to the 2D section of the 3D object using a light source. For the subsequent layers, the process proceeds until the completion of the object by repeating the sequence of lowering the build platform by a specific quantity equal to the set layer thickness, distributing the powder and exposing the material using the energy source. To promote the sintering and component geometry stability, the chamber and the powder bed are kept at a temperature nearly equal to the polymer glass transition temperature [17]. Because of that, at the end of the process, the object is surrounded by sintered powder that must be removed by a mechanical action, such as shot peening [18]. The presence of sintered material surrounding the object may inhibit the fabrication of intricate structures because of the difficulties in accessing the smaller pores or the central part of the structure to remove the sintered powder [19].

The samples made by TPU, with the commercial name of ESTANE® 3D TPU M95A [20], were processed via the HP® JetFusion 4200 MultiJetFusion. This system uses an infrared light to sinter the material. To accelerate the sintering process, before the exposure, the powder material is wetted by a so-called fusing agent [21]. The percentage of irradiance was set equal to -2%. The remaining process

parameters are closed; therefore, they were pre-set for the selected material as suggested by the supplier.

The samples made in PA12, commercially PA2200 [22], were produced using a Formiga Velocis P110 (EOS GmbH). This system employs a CO₂ laser of 21 W to sinter the powder. The temperature levels of the removal chamber and process chamber were set to 154 °C and 172 °C, respectively.

In both systems, a layer thickness of 0.1 mm was set.

For each configuration, three replicas were manufactured and tested. Figure 2 shows the four specimen configurations produced in PA12 and TPU compared to the nominal CAD. The variation of the L and D parameters highlights the differences in volume fraction.

As mentioned above, a multi-cell configuration was designed to emulate the crashworthiness capabilities of the structure during a real application as the padding shell element (also known as liner) of a helmet. Considering the typical thickness of a liner (40 mm), the L20_D1.6 configuration was selected to be replicated in a matrix arrangement 2×2×2, as depicted in Fig. 3. The multi-cells, named L20_D1.6_2×2×2, was manufactured only in TPU material. Since the replication transformation is required to maintain the minimum gap among the adjacent replicas to avoid obstruction during the bending movements, the volume envelope of the structure increased, generating a reduced value of VF (16%) compared to the unitarian cell (20.1%).

Quasi-static tests were performed using a Shimadzu universal testing machine with a 5 kN load cell at a 1 mm/min speed. The high-speed (HS) compression load tests were performed using an in-house drop tower system developed at the University of Aveiro. The schematic representation of the drop tower machine is illustrated in Fig. 4. The impactor displacement was measured using a positional encoder (from where strains were calculated), whereas the response force related to the impact was measured using a 20 kN load cell. The impactor assembly (Fig. 4), containing the load cell, has a total mass of 20 kg. The flat square surface of the impactor (130 mm side length) guarantees a uniform application of the load on the specimen upper surface.

The specimens characterised by the lower value of VF, i.e., the L40_D2.0, were used to conduct a preliminary characterisation of the structure under

Table 1 Material and mechanical properties of the PA2200 (PA12) [22] and ESTANE® 3D TPU M95A-545 powders (TPU) [20] according to the technical datasheet

	PA2200	ESTANE® 3D TPU M95A
Tensile modulus (MPa)	1650	60
Tensile strength (MPa)	48	11
Elongation at break (%)	18	180
Melting temperature (°C)	176	200
Bulk density (g/cm ³)	0.45	N/A
Sintered part density (g/cm ³)	0.93	1.17

Fig. 2 3D-CFS configurations with related VF: from top to bottom CAD version design, PA12 and TPU manufactured specimens

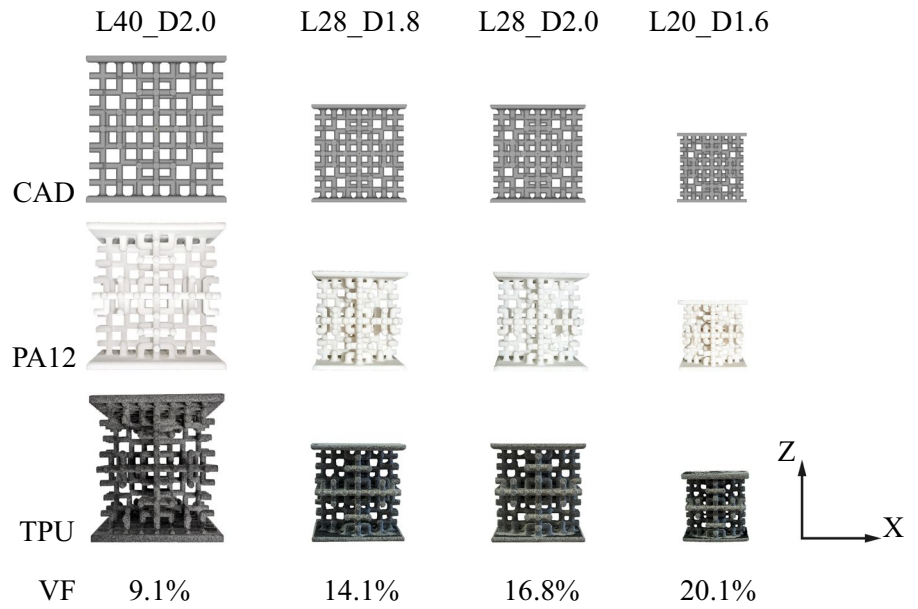
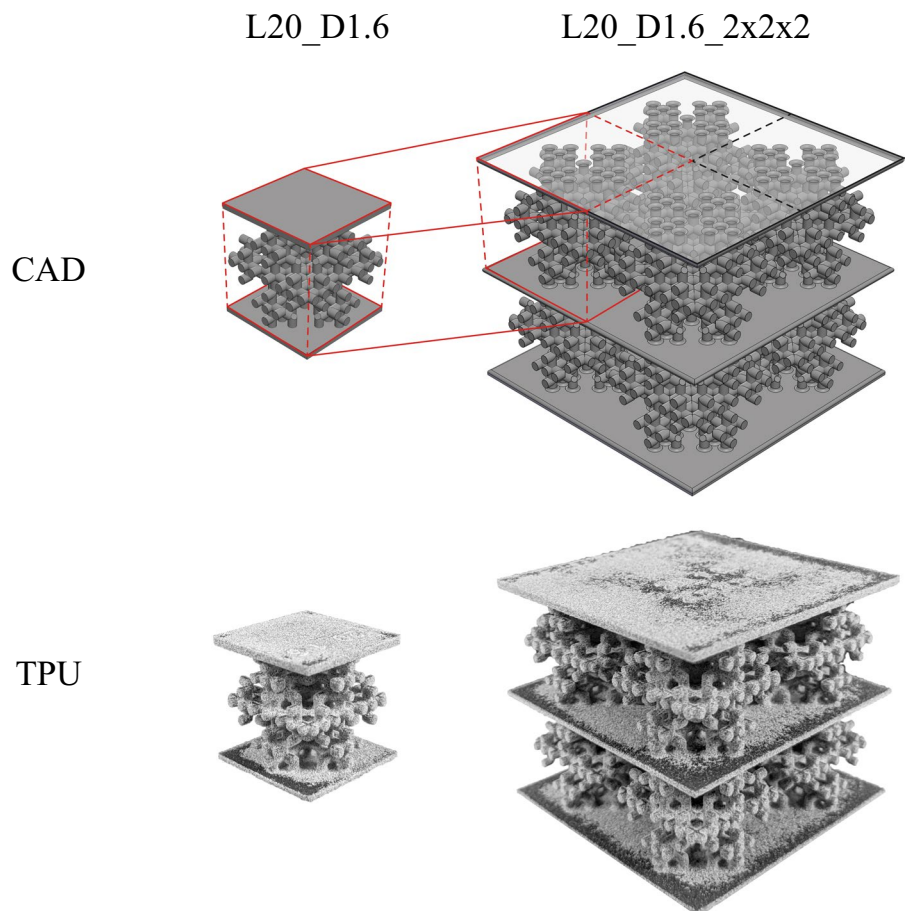


Fig. 3 Single and multiple-cell configuration of the sample L20_D1.6. Top: CAD illustration; bottom: representation of the TPU-manufactured samples



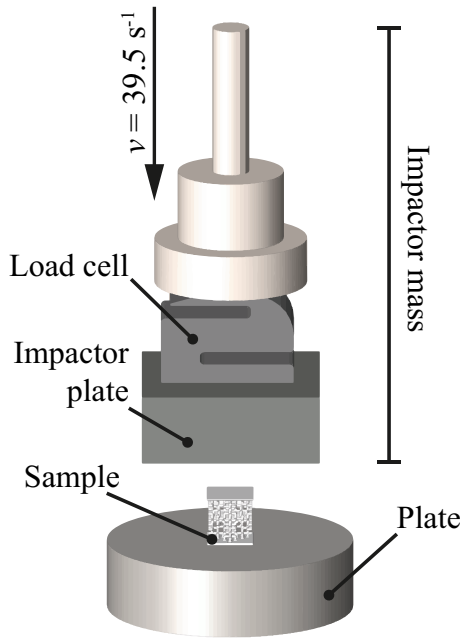


Fig. 4 Schematic illustration of the drop tower system employed for the high-speed impact tests

a pre-set impact energy quantity value equal to 50 J. This test revealed that the selected energy was too high to detect the structure response adequately; therefore, the energy was subsequently reduced to 25 J, except for the multiple-cell configuration. The resulting strain rates at the impact onset were 55.9 s^{-1} for the first test (50 J) and 39.5 s^{-1} for the subsequent test with 25 J. As an example, a video recording showing the experimental test of the multiple-cell

configuration tested under 25 J impact load was provided as a supplementary file.

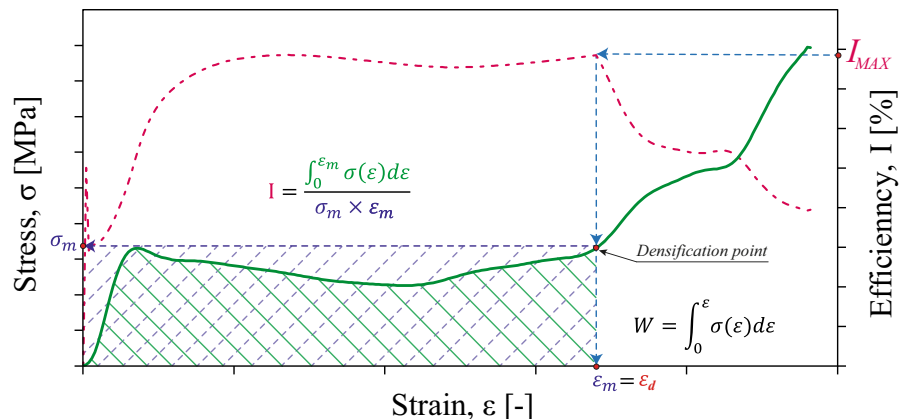
From the test, the measurements were elaborated to quantify the energy absorption properties of the structures using the energy per unit volume (W). This index was obtained by measuring the portion of the area subtended from the stress–strain curve at the densification point (ϵ_d), as illustrated in Fig. 5. The ϵ_d point for each structure was determined by identifying the strain point corresponding to the highest value of the Ideality (I) efficiency parameter (see Fig. 5) for the investigated absorber. I is obtained by comparing the performance of the actual tested material with the corresponding of an ideal absorber. Thus, as observed in the formula reported in Fig. 5, the Ideality parameter is calculated as the ratio between the energy per unit volume evaluated up to the ϵ_d (W_{ϵ_d}) and the ideal energy per unit volume, i.e., the product between the stress at the densification point ($\sigma_m = \sigma_{\epsilon_d}$) and ϵ_d [23].

In addition, since the materials employed in this study have different density values (Table 1), to make them comparable, the properties W has been divided by the material density, obtaining the so-called specific energy absorption (SEA).

3 Results and discussion

As mentioned above, the preliminary test was performed with an impact energy equal to 50 J. Figure 6a shows the results from the impact tests of L40_D2.0 for PA12 and TPU. The difference in stresses between the two materials is relevant. Specifically, the first response to the impact mass shown in the curve

Fig. 5 Evaluation of the densification point through the Efficiency I curve (dotted red curve). The area under the stress vs. strain curve (green line) highlighted in green represents W . The dotted purple area refers to the ideal amount of energy absorption up to the ϵ_d



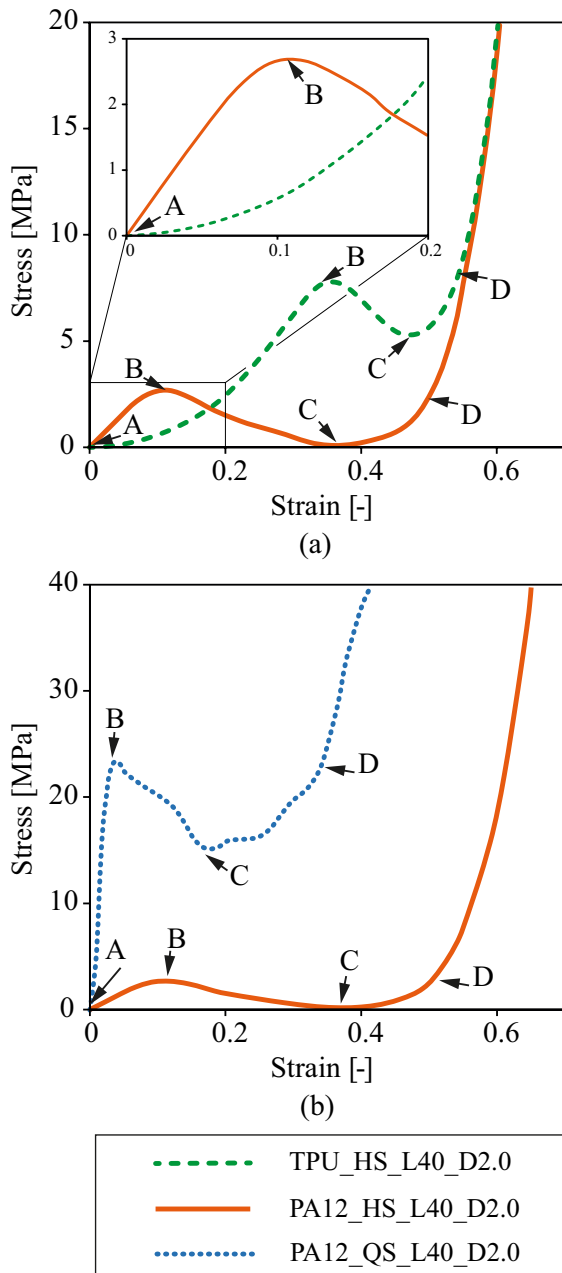


Fig. 6 Strain vs. stress curves of L40_D2.0 specimen: **a** comparison between the 3D-CFS manufactured with PA12 and TPU and tested with high-speed compression load (50 J); **b** comparison between the L40_D2.0 made in PA12 and tested with a quasi-static and high-speed compression load

elastic region (Segment AB in Fig. 6) reveals that, despite the higher stiffness of the PA12 sample, the elasticity of the TPU counterpart accommodates better the strut bending behaviour by reaching a higher

value of strain before the plastic region (Point B in Fig. 6). Then, after the quasi-linearly bending and the material has reached peak B in Fig. 6, a quick collapse can be observed (point C in Fig. 6), probably due to premature failure of some struts or multiple fractures in the structure [5]. After the collapse of the struts, the structure densifies, as can be noticed by the rapid increase of the stress without increasing the strain (Point D in Fig. 6). This behaviour is most appreciable when the dependency of the material behaviour from the strain rate is higher, especially in brittle materials such as the PA12 processed by PBF [21]. This aspect could be easily detected by comparing the compression curves of the same 3D-CFS tested with quasi-static and dynamic load (Fig. 6b). The fracture mechanism shown by the sample tested under HS load significantly decreases the structure strength response. In contrast, the QS sample showed more controlled deformation mechanisms that guarantee handling more stress before densification.

Considering the findings mentioned above, the other structures were tested at lower impact energy equal to 25 J.

Figures 7, 8, and 9 report the results of the impact tests performed on the L28_D1.8, L28_D2.0, and L20_D1.6 specimens, respectively.

As it can be observed, the stress and strain values among the replicas were quite similar. However, the deviations in the deformation mechanisms were significantly different, especially for the PA12 specimens. The observed deviations may be attributed to defects induced during the manufacturing process, which can result in various localised fractures of the struts [24, 25].

Compared to L40_D2.0, the 3D-CFS configurations with L = 28 mm showed higher energy absorption values with a notable plateau region for both materials. Owing to the lower stiffness, the energy absorption characteristics of TPU are relatively lower than those of PA12 specimens. Conversely, the magnitude of stress within the initial phase of impact is considerably reduced.

Regarding L20_D1.6, the results shown in Fig. 9 indicate that the structure experiences rapid densification in response to the impact. This behaviour is caused by the high volume fraction of the geometry, which limits the bending of the strut and generates a rapid increase in the force response, reducing the structure capability to absorb the energy uniformly.

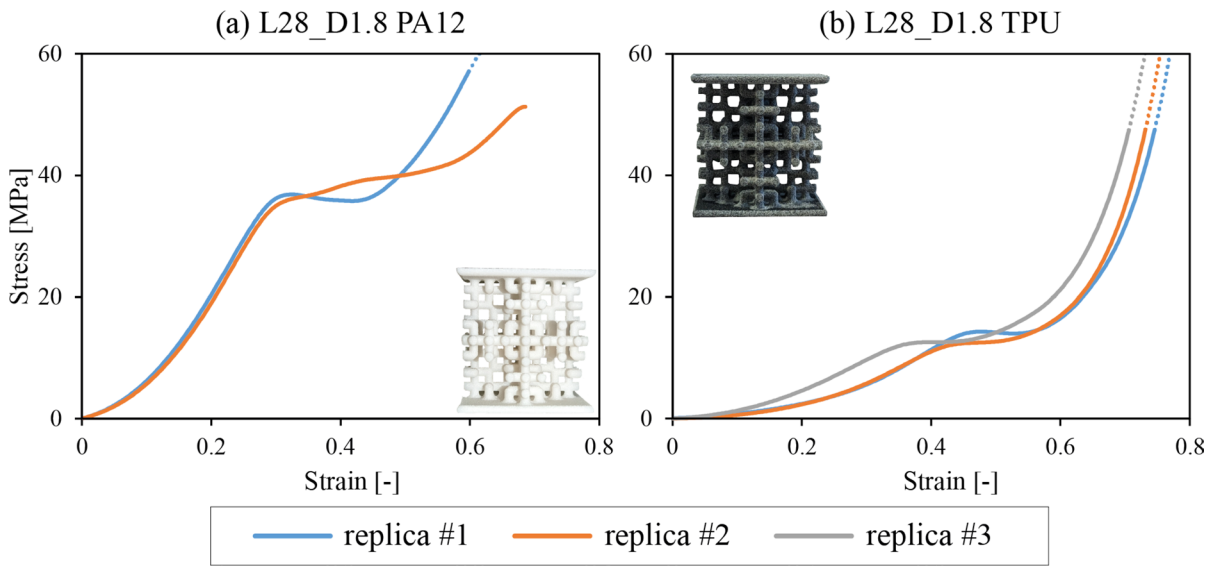


Fig. 7 Strain vs. stress curves of all the replicas of L28_D1.8 (VF=14.1%) configuration manufactured in PA12 (a) and TPU (b) materials and tested under high-speed impact load (25 J)

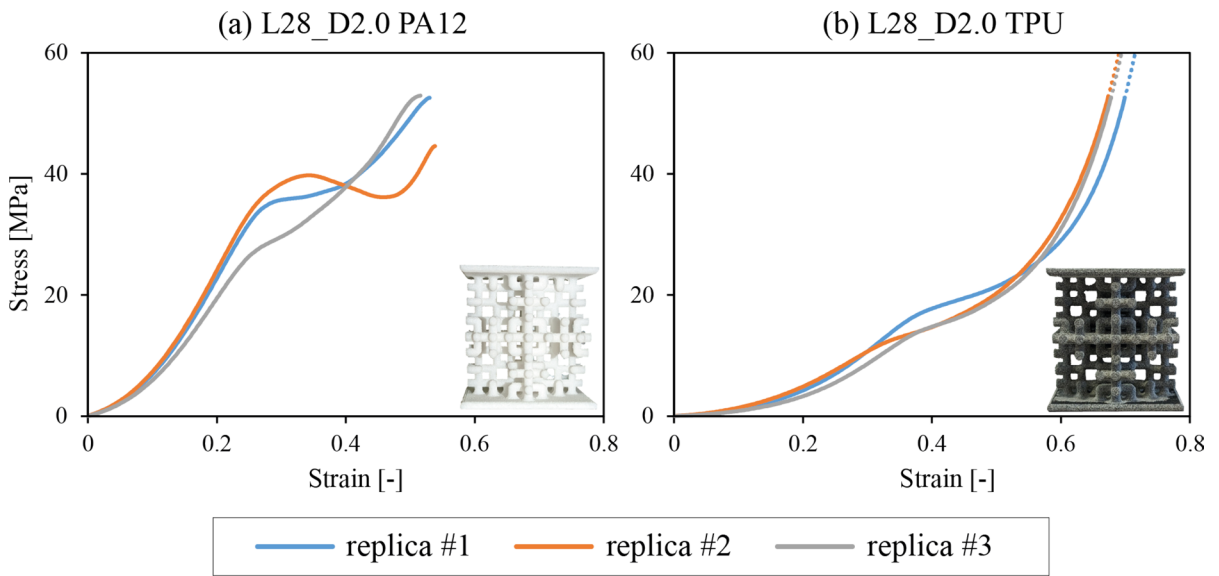


Fig. 8 Strain vs. stress curves of all the replicas of L28_D2.0 (VF=16.8%) configuration manufactured in PA12 (a) and TPU (b) materials and tested under high-speed impact load (25 J)

The phenomenon is particularly pronounced in the TPU samples, as the lower stiffness leads to a rapid collapse, resulting in a consistent increase in the compression curve response.

However, in the multi-cell arrangement, which was tested with the same impact load (25 J) as the related single cell, the energy absorption performances increased significantly (Fig. 10a). As evidenced by the video recording that is included as a

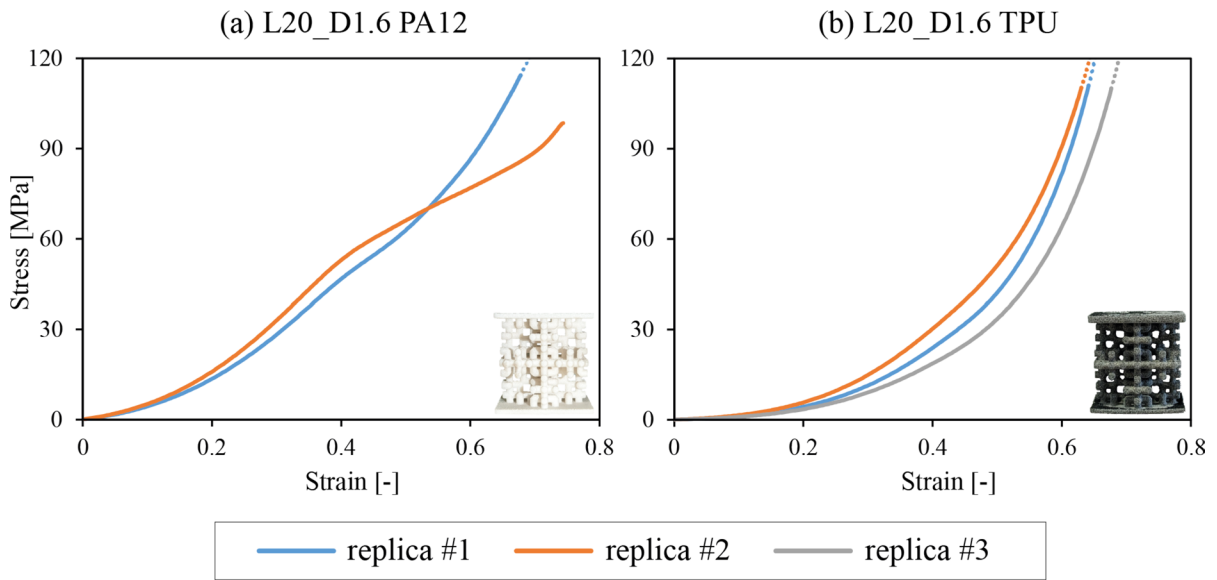


Fig. 9 Strain vs. stress curves of all the replicas of L20_D1.6 (VF=20.1%) configuration manufactured in PA12 (a) and TPU (b) materials and tested under high-speed impact load (25 J)

supplementary file, the larger surface of the top plate guarantees the distribution of the impact load among the eight replicas of the L20_D1.6 uniformly, enabling them to reach deformation mechanisms close to the those observed in the single structure configuration [15] and generating an extended plateau region, that means higher energy absorption. Furthermore, when examining the acceleration vs. time graph depicted in Fig. 10b, it becomes more evident that the multiple-cell structures possess superior absorption capabilities. Particularly, an ideal absorber should maintain the peak of acceleration (PA) low as soon as possible and dissipate the impact energy for a long time to avoid damage to the protected item. As the graphs show, the PA of the L20_D1.6_2×2×2 samples (20.7 ± 0.9 g) are significantly lower than the L20_D1.6 (24.2 ± 1 g). In addition, the energy dissipation time of the multiple-cell structure is double that of the single-cell.

From the HS compression tests, all the parameters extracted (σ_{ed} and ϵ_d) and calculated (W_{ed} , SEA, I) are reported in Table 2. The structures made by PA12 performed better than TPU counterparts in terms of SEA and I. In comparison with the set corresponding to L=28 mm, a lower VF promoted a slightly better absorption efficiency. This result is due to the lower

stress obtained at the densification point. Owing to the rapid densification mainly observed in structures with too low or too high volume fraction, e.g. L40_D2.0 and L20_D1.6 configurations, respectively, the measured values of Ideality are significantly lower than the other structures.

The configuration using multiple cells enhanced the performance with respect to the single structures, reaching an efficiency parameter of 52%. Regarding SEA, it appears that L20_1.6 tested in single-cell performed better than multiple-cell configuration. However, it should be observed that by definition (See Sect. 2.2), the SEA considers the densification of the structure and, therefore, is affected by the higher stress detected for the single cell. On the other hand, in that condition, the structure already failed; when densified, it cannot dissipate energy efficiently. Conversely, the I descriptor reveals how the multiple-cell configuration dissipates the energy generated during the impact better thanks to the deformability of the internal reticular structure, which occurs under a more controlled and slow bending mechanism. This absorbed energy via the controlled deformation allows the multi-cell configuration to be more suitable for damage reduction, e.g., in the case of an application for personal

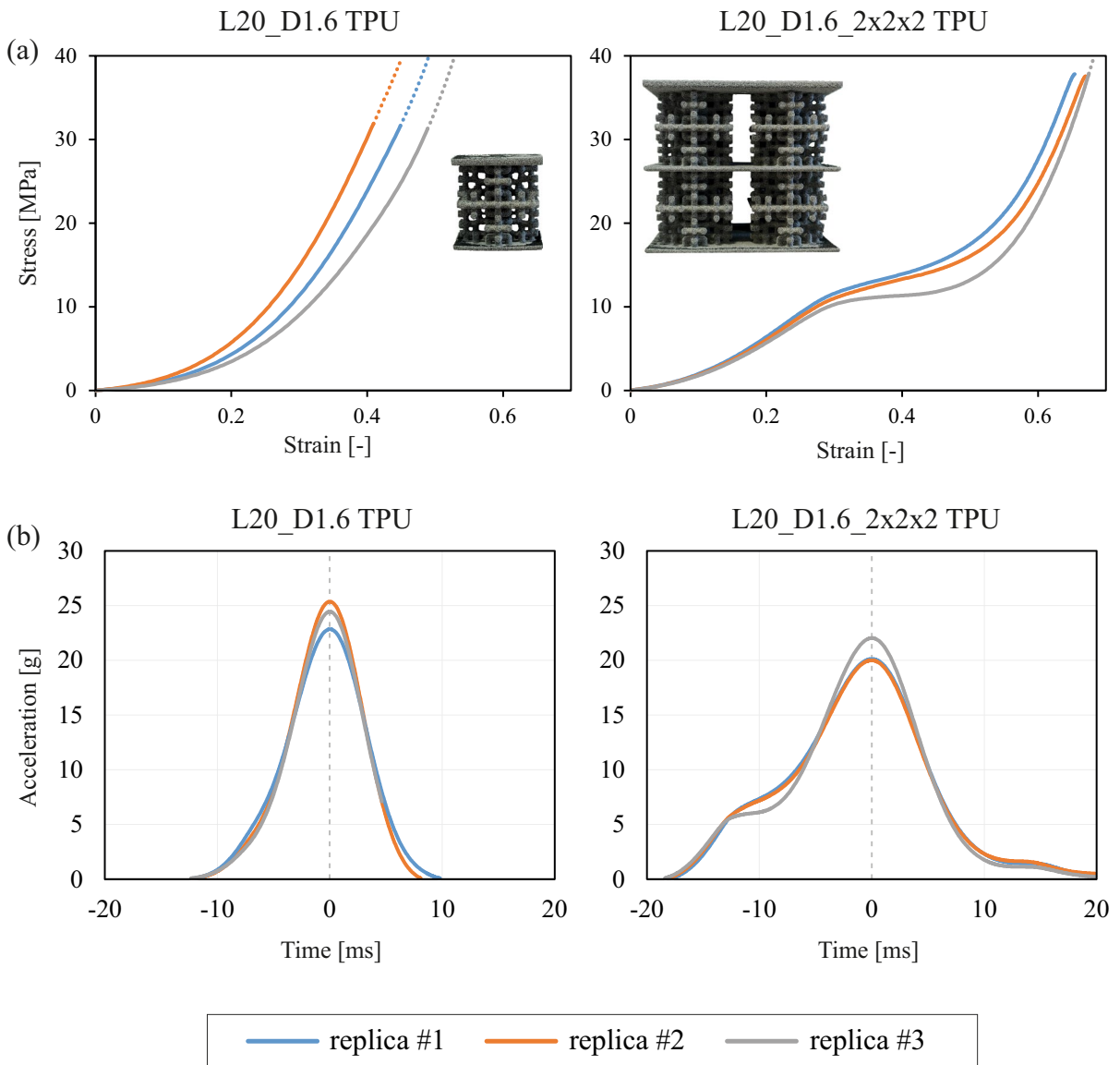


Fig. 10 Comparison of the energy absorption performance between the L20_D1.6 (VF=20.1%) and the L20_D1.6_2x2x2 (VF=16%) manufactured with TPU material; **a**

strain vs. stress curves and **b** acceleration vs. time graph of all the replicas for each configuration

protective equipment head protection. In this regard, data on the high strain rate response of complex structures produced by AM are lacking. Compared with the available data for cellular structures [5, 26, 27], the efficiency of the 3D-CFS structure is comparable or slightly lower, while the SEA parameter is significantly higher (up to six times in the case of 3D-CFS multiple cells) and comparable to the traditional foam obtained by moulding [28].

4 Conclusions

This study aims to examine the energy absorption capabilities of 3D-CFS under high-speed compression loads. The structures were fabricated using two polymeric materials, PA12 and TPU, through the powder bed fusion technique. Different structures have been designed by varying the length and the diameter of the beam initiator to obtain structures with different

Table 2 Energy absorption indicators for the PA12 and TPU structures with different volume fractions (VF) under high-speed compression loads. Standard deviation in brackets

	L40_D2.0*		L28_D1.8		L28_D2.0		L20_D1.6		L20_D1.6_2×2×2
VF (%)	9.1		14.1		16.8		20.1		16
	PA12	TPU	PA12	TPU	PA12	TPU	PA12	TPU	TPU
σ_{ed} (MPa)	2.8	7.9	39.7 (1.3)	13.9 (0.5)	38.6 (1.3)	19.5 (2.6)	75.8 (11)	35.3 (0.6)	14.1 (1.5)
ε_d (%)	51	55	52 (3)	53 (3)	44 (5)	49 (3)	59 (1)	47 (1)	46 (1)
W_{ed} (MJ/m ³)	0.59	2.17	12.6 (1.2)	3.4 (0.2)	9.7 (2.5)	3.9 (0.8)	20.8 (8)	4.9 (0.9)	3.4 (0.2)
SEA (kJ/kg)	0.64	1.98	13.6 (1.3)	3.1 (0.2)	10.4 (2.7)	3.5 (0.7)	23.1 (9)	4.4 (0.8)	3.1 (0.2)
I (%)	41	51	61 (0.3)	46 (0.3)	56 (6)	41 (2)	44 (4)	29 (0.7)	52 (2.5)

*For L40_D2.0, only a replica has been tested at HS to adjust the impact energy level for the subsequent tests

volume fractions. Also, a new layout, including multiple cells, has been designed to emulate the crashworthiness capabilities of an actual application.

The test results have shown that the behaviour of both PA12 and TPU samples is significantly strain-rate dependent. Overall, the volume fraction range that can provide higher efficiency values in terms of energy absorption of 3D-CFS under high strain rate has been identified between 14 and 17%. The multiple-cell configuration showed an excellent energy absorption value with low values of the acceleration peak compared to the related unitarian cell. PA12 3D-CFS is a high energy absorber, but the TPU 3D-CFS ensures a significantly lower peak for the force impact. In the case of applications for personal protective equipment, the performance of TPU may be ideal for avoiding brain injuries during the impact. However, this could not be enough if the percentage of energy absorbed at the impact is low. Therefore, a possible solution could be to combine the two materials with a proper design in which the capabilities revealed could be exploited.

Author contributions M. V.: data curation, formal analysis, investigation, methodology, validation, visualisation, writing (original draft); G. S.: investigation; R. A. S.: resources, supervision, writing (review and editing); M. G.: conceptualisation, methodology, resources, supervision, writing (review and editing). All authors have read and agreed to the published version of the manuscript.

Funding Open access funding provided by Politecnico di Torino within the CRUI-CARE Agreement.

Data availability The data that support the findings of this study are available upon reasonable request.

Declarations

Conflict of interest The authors declare that they have no conflict of interest.

Ethical approval Not applicable.

Open Access This article is licensed under a Creative Commons Attribution 4.0 International License, which permits use, sharing, adaptation, distribution and reproduction in any medium or format, as long as you give appropriate credit to the original author(s) and the source, provide a link to the Creative Commons licence, and indicate if changes were made. The images or other third party material in this article are included in the article's Creative Commons licence, unless indicated otherwise in a credit line to the material. If material is not included in the article's Creative Commons licence and your intended use is not permitted by statutory regulation or exceeds the permitted use, you will need to obtain permission directly from the copyright holder. To view a copy of this licence, visit <http://creativecommons.org/licenses/by/4.0/>.

References

1. Rice University, Rice tapped to develop 3D-printed 'smart helmets' for the military, (n.d.)
2. Khosroshahi SF, Olsson R, Wysocki M, Zaccariotto M, Galvanetto U (2018) Response of a helmet liner under biaxial loading. *Polym Test* 72:110–114. <https://doi.org/10.1016/j.polymertesting.2018.10.012>
3. Gao W, He X, Wang J, Feng YT, Wang C (2022) Numerical investigation of oblique impact behavior of a helmeted headform on a windshield considering failure. *Thin-Walled Struct* 171:108722. <https://doi.org/10.1016/j.tws.2021.108722>
4. Jhou SY, Hsu CC, Yeh JC (2021) The dynamic impact response of 3d-printed polymeric sandwich structures with lattice cores: numerical and experimental

- investigation. *Polymers* (Basel). <https://doi.org/10.3390/polym13224032>
5. Sun ZP, Guo YB, Shim VPW (2022) Static and dynamic crushing of polymeric lattices fabricated by fused deposition modelling and selective laser sintering – an experimental investigation. *Int J Impact Eng* 160:104059. <https://doi.org/10.1016/j.ijimpeng.2021.104059>
 6. Ramos H, Santiago R, Soe S, Theobald P, Alves M (2022) Response of gyroid lattice structures to impact loads. *Int J Impact Eng* 164:104202. <https://doi.org/10.1016/j.ijimpeng.2022.104202>
 7. Syam WP, Jianwei W, Zhao B, Maskery I, Elmadih W, Leach R (2018) Design and analysis of strut-based lattice structures for vibration isolation. *Precis Eng* 52:494–506. <https://doi.org/10.1016/j.precisioneng.2017.09.010>
 8. Miralbes R, Higuera S, Ranz D, Gomez JA (2021) Comparative analysis of mechanical properties and energy absorption capabilities of functionally graded and non-graded thermoplastic sheet gyroid structures. *Mech Adv Mater Struct*. <https://doi.org/10.1080/15376494.2021.1949509>
 9. Maconachie T, Leary M, Lozanovski B, Zhang X, Qian M, Faruque O, Brandt M (2019) SLM lattice structures: properties, performance, applications and challenges. *Mater Des* 183:108137. <https://doi.org/10.1016/J.MATDES.2019.108137>
 10. Wang J, Zhang Y, He N, Wang CH (2018) Crashworthiness behavior of Koch fractal structures. *Mater Des* 144:229–244. <https://doi.org/10.1016/j.matdes.2018.02.035>
 11. Zhang Y, Wang J, Wang C, Zeng Y, Chen T (2018) Crashworthiness of bionic fractal hierarchical structures. *Mater Des* 158:147–159. <https://doi.org/10.1016/j.matdes.2018.08.028>
 12. Zhang Y, He N, Song X, Chen T, Chen H (2020) On impacting mechanical behaviors of side fractal structures. *Thin-Walled Struct* 146:106490. <https://doi.org/10.1016/j.tws.2019.106490>
 13. Mehta PS, Solis Ocampo J, Tovar A, Chaudhari P (2016) Bio-inspired design of lightweight and protective structures, SAE Technical Paper. <https://doi.org/10.4271/2016-01-0396>.
 14. Najmon JC, Dehart J, Wood Z, Tovar A (2018) Cellular helmet liner design through bio-inspired structures and topology optimization of compliant mechanism lattices. *SAE Int J Transp Saf* 6:217–235. <https://doi.org/10.4271/2018-01-1057>
 15. Viccica M, Galati M, Calignano F, Iuliano L (2022) Design, additive manufacturing, and characterisation of a three-dimensional cross-based fractal structure for shock absorption. *Thin-Walled Struct*. 181:110106. <https://doi.org/10.1016/j.tws.2022.110106>
 16. Viccica-Marcorra GF, Fernandes F, Calignano F, Iuliano L, de Sousa RA, Galati M (2023) Characterisation of an additively manufactured 3d cross-based fractal structure for impact energy absorption. In: Gabriele S, Manuello-Bertetto A, Marmo F, Micheletti A (eds) *Shell Spat Struct IWSS 2023 Lecture Notes Civil*. Springer Nature, Cham, pp 454–461. https://doi.org/10.1007/978-3-031-44328-2_47
 17. Hassan MS, Billah KMM, Hall SE, Sepulveda S, Regis JE, Marquez C, Cordova S, Whitaker J, Robison T, Keating J, Shafirovich E, Lin Y (2022) Selective laser sintering of high-temperature thermoset polymer. *J Compos Sci*. <https://doi.org/10.3390/jcs6020041>
 18. Cai C, Tey WS, Chen J, Zhu W, Liu X, Liu T, Zhao L, Zhou K (2021) Comparative study on 3D printing of polyamide 12 by selective laser sintering and multi jet fusion. *J Mater Process Technol* 288:116882. <https://doi.org/10.1016/j.jmatprotec.2020.116882>
 19. Rodríguez-Aparicio R, Alegre JM, Verbeeten WMH, Lorenzo-Bañuelos M, Cuesta II (2023) Methodology to predict mechanical properties of Pa-12 lattice structures manufactured by powder bed fusion. *Addit Manuf* 78:103864. <https://doi.org/10.1016/j.addma.2023.103864>
 20. Lubrizol Estane 3D TPU datasheet (2021)
 21. Galati M, Calignano F, Defanti S, Denti L (2020) Disclosing the build-up mechanisms of multi jet fusion: experimental insight into the characteristics of starting materials and finished parts. *J Manuf Process* 57:244–253. <https://doi.org/10.1016/j.jmapro.2020.06.029>
 22. EOS GmbH - Electro Optical Systems, Material data sheet PA 2200, (2017)
 23. Miralbes R, Ranz D, Ivens J, Gomez JA (2021) Characterization of cork and cork agglomerates under compressive loads by means of energy absorption diagrams. *Eur J Wood Wood Prod* 79:719–731. <https://doi.org/10.1007/s00107-020-01625-7>
 24. Calignano F, Giuffrida F, Galati M (2021) Effect of the build orientation on the mechanical performance of polymeric parts produced by multi jet fusion and selective laser sintering. *J Manuf Process* 65:271–282. <https://doi.org/10.1016/j.jmapro.2021.03.018>
 25. Galati M, Viccica M, Minetola P (2021) A finite element approach for the prediction of the mechanical behaviour of layered composites produced by continuous filament fabrication (CFF). *Polym Test*. <https://doi.org/10.1016/j.polymertesting.2021.107181>
 26. Habib FN, Iovenitti P, Masood SH, Nikzad M (2018) Cell geometry effect on in-plane energy absorption of periodic honeycomb structures. *Int J Adv Manuf Technol* 94:2369–2380. <https://doi.org/10.1007/s00170-017-1037-z>
 27. Habib F, Iovenitti P, Masood S, Nikzad M, Ruan D (2019) Design and evaluation of 3D printed polymeric cellular materials for dynamic energy absorption. *Int J Adv Manuf Technol* 103:2347–2361. <https://doi.org/10.1007/s00170-019-03541-4>
 28. de Sousa RA, Coelho R, Teixeira-Dias F, Gonçalves D (2012) Assessing the effectiveness of a natural cellular material used as safety padding material in motorcycle helmets. *SIMULATION* 88:580–591. <https://doi.org/10.1177/0037549711414735>

Publisher's Note Springer Nature remains neutral with regard to jurisdictional claims in published maps and institutional affiliations.